



Cite this: *Chem. Commun.*, 2022, 58, 11917

Received 5th September 2022,
Accepted 22nd September 2022

DOI: 10.1039/d2cc04912k

rsc.li/chemcomm

Long-lived photoluminescence from an eight-coordinate zirconium(IV) complex with four 2-(2'-pyridyl)pyrrolide ligands[†]

Dylan C. Leary, Jordan C. Martinez, Novruz G. Akhmedov, Jeffrey L. Petersen and Carsten Milsmann *

The photoluminescent eight-coordinate zirconium complex $\text{Zr}^{(\text{H}\text{PMP}^{\text{H}})}_4$ supported by four monoanionic 2-(2'-pyridyl)pyrrolide ligands was synthesized. This molecule shows dual emission *via* fluorescence and phosphorescence with an overall quantum efficiency of 4% at room temperature in solution. The phosphorescence lifetime is dependent on concentration, indicating excimer formation at higher concentrations, and reaches almost 800 μs at high dilution.

The broad utility of photosensitizers in applications such as dye-sensitized solar cells,¹ organic light-emitting diodes (OLEDs),^{2,3} and photocatalysis^{4,5} makes them diverse tools available to the scientific community. Molecular transition-metal photosensitizers have traditionally relied on precious 2nd and 3rd row metals, most prominently ruthenium and iridium, whose scarcity,⁶ coupled with a global effort towards more sustainable chemistry, encourages the development of more environmentally friendly alternatives.

Inspired by their precious metal counterparts, work on Earth-abundant photoluminescent transition-metal complexes has with few exceptions⁷ focused on electron-rich 1st row transition metals that allow access to metal-to-ligand charge transfer (MLCT) excited states.^{8–10} A major challenge in these systems arises from the smaller ligand-field splitting in 1st row transition metals that leads to low-lying metal-centred (MC) excited states. These states provide a pathway for facile non-radiative decay,¹¹ resulting in significantly shorter excited state lifetimes and poor photoluminescence quantum yields. While recent work employing strong-field ligands has shown promise for circumventing excited-state deactivation in 3d⁶ emitters,^{12–16} the complete elimination of MC excited states in copper(I) systems with 3d¹⁰ ground state configurations has made them

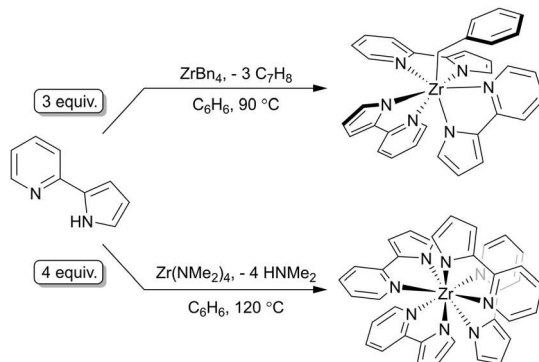
the most popular Earth-abundant alternative to precious metal photosensitizers.¹⁷

A fundamentally different but equally promising strategy to prevent MC excited states altogether is considering d⁰ metal centres. Supporting early transition metals with electron-rich ligands has resulted in the development of photoluminescent complexes whose excited-state manifold is based on ligand-to-metal charge transfer (LMCT).^{18–20} In this arena, we have shown that the complexes $\text{Zr}^{(\text{R}^1\text{PDP}^{\text{R}^2})}_2$ ($[\text{R}^1\text{PDP}^{\text{R}^2}]^{2-}$ = 2,6-bis(5-R₁-3-R₂-pyrrol-2-ide)pyridine) exhibit strong photoluminescence *via* thermally activated delayed fluorescence (TADF) with lifetimes in the microsecond range and are competent photosensitizers for applications in visible light photoredox catalysis^{21–23} and photon upconversion.²⁴

Inspired by the success of pyridine dipyrrolide ligands, we recently employed a related monoanionic pyridine monopyrrolide ligand in the series $\text{M}^{(\text{Me}\text{PMP}^{\text{Me}})}_3\text{Cl}$ ($\text{M} = \text{Zr, Hf}$; $[\text{Me}\text{PMP}^{\text{Me}}]^{1-}$ = 3,5-dimethyl-2-(2'-pyridyl)pyrrolide).²⁵ These seven-coordinate complexes exhibit visible-light induced photoluminescence, proposed to result from dual emission *via* fluorescence and phosphorescence pathways. However, it was shown that their structural flexibility provides pathways for facile non-radiative decay manifested in poor photoluminescence quantum yields ($\Phi_{\text{PL}} \leq 0.01$). Furthermore, the relatively open coordination sphere around zirconium leaves the $\text{Zr}-\text{N}_{\text{pyrrolide}}$ bonds vulnerable to hydrolysis, which makes the complexes unstable to residual air or moisture. We hypothesized that both drawbacks could be addressed by coordinatively saturating the zirconium centre with another $[\text{PMP}]^{1-}$ unit. Due to the increased steric congestion around the zirconium centre, the proposed eight-coordinate species should be more rigid, resulting in reduced non-radiative relaxation, and less prone to $\text{Zr}-\text{N}_{\text{pyrrolide}}$ bond hydrolysis. In this work, we demonstrate that the use of unsubstituted (2-pyridyl)pyrrolide ligands, $[\text{H}\text{PMP}^{\text{H}}]^{1-}$, allows facile synthetic access to the air-stable, photoluminescent complex $\text{Zr}^{(\text{H}\text{PMP}^{\text{H}})}_4$, which shows improved optical properties compared to the seven-coordinate species $\text{Zr}(\text{PMP})_3\text{X}$ ($\text{X} = \text{Cl, benzyl}$).

C. Eugene Bennett Department of Chemistry, West Virginia University, 100 Prospect Street, Morgantown, WV 26505, USA. E-mail: camilsmann@mail.wvu.edu

† Electronic supplementary information (ESI) available. CCDC 2205413 and 2205414. For ESI and crystallographic data in CIF or other electronic format see DOI: <https://doi.org/10.1039/d2cc04912k>



Scheme 1 Synthesis of the two zirconium complexes discussed in this study.

In pursuit of $\text{Zr}(\text{H}\text{PMPH})_4$, four equivalents of $\text{H}^{\text{H}}\text{PMPH}$ ($\text{H}^{\text{H}}\text{PMPH} = 2\text{-}(2'\text{-pyridyl})\text{pyrrole}$) were heated at $90\text{ }^{\circ}\text{C}$ with one equivalent of tetrabenzyl zirconium. Despite this particular stoichiometry, the seven-coordinate complex $\text{Zr}(\text{H}\text{PMPH})_3\text{Bn}$ was isolated (Scheme 1) in 90% yield as the only metal-containing product. Heating $\text{Zr}(\text{H}\text{PMPH})_3\text{Bn}$ in the presence of excess $\text{H}^{\text{H}}\text{PMPH}$ at temperatures greater than $90\text{ }^{\circ}\text{C}$ provided no further reaction towards the desired eight-coordinate $\text{Zr}(\text{H}\text{PMPH})_4$. Single crystal X-ray diffraction (Fig. S1, ESI[†]) revealed a C_1 -symmetric, seven-coordinate structure for $\text{Zr}(\text{H}\text{PMPH})_3\text{Bn}$ directly analogous to $\text{Zr}(\text{Me}\text{PMPMe})_3\text{Cl}$.²⁵ The $\text{Zr}-\text{CH}_2-\text{C}_{ipso}$ angle of $114.6(4)^{\circ}$ and long $\text{Zr}-\text{C}_{ipso}$ distance of $3.180(5)\text{ \AA}$ indicate the benzyl group is η^1 -bound²⁶ which contrasts the η^2 -benzyl binding motif in recently reported $\text{Zr}(\text{Me}\text{PMPMe})_3\text{Bn}_2$.²⁷ Similar to $\text{Zr}(\text{Me}\text{PMPMe})_3\text{Cl}$, the structure of $\text{Zr}(\text{H}\text{PMPH})_3\text{Bn}$ in solution is highly flexible, which was established by variable-temperature (VT) NMR spectroscopy between $-58\text{ }^{\circ}\text{C}$ and $+70\text{ }^{\circ}\text{C}$ in toluene- d_8 (Fig. S2 and S3, ESI[†]). While a C_1 -symmetric structure consistent with the crystallographic data is observed at low temperatures, a rapid dynamic process with an estimated energetic barrier of $\Delta G^{\ddagger} = 16.4\text{ kcal mol}^{-1}$ renders all three $[\text{H}\text{PMPH}]^{1-}$ ligands equivalent on the NMR timescale at and above room temperature, resulting in apparent C_3 symmetry for the molecule (see ESI[†] for details). No photophysical data were collected for $\text{Zr}(\text{H}\text{PMPH})_3\text{Bn}$ because the complex undergoes rapid decomposition under ambient light (Fig. S13, ESI[†]), likely due to photolysis of the zirconium-benzyl bond.

In an attempt to reduce the steric profile of the zirconium starting material and eliminate the presence of temperature- and light-sensitive Zr-benzyl moieties, $\text{Zr}(\text{NMe}_2)_4$ was identified as a potentially more suitable precursor to $\text{Zr}(\text{H}\text{PMPH})_4$. Reaction of 4 equivalents of $\text{H}^{\text{H}}\text{PMPH}$ with 1 equivalent of $\text{Zr}(\text{NMe}_2)_4$ at $120\text{ }^{\circ}\text{C}$ (Scheme 1) provided the air- and moisture-stable $\text{Zr}(\text{H}\text{PMPH})_4$ as a yellow crystalline solid in 88% yield. The molecule crystallizes in the monoclinic space group C_2/c with a crystallographic C_2 axis passing through the zirconium centre (Fig. 1). The $\text{Zr}-\text{N}_{\text{pyrrole}}$ distances ($2.2272(9)$ and $2.2344(9)\text{ \AA}$) are similar to other reported $\text{Zr}(\text{PMP})_m\text{X}_n$ complexes^{23,25} while the $\text{Zr}-\text{N}_{\text{pyridine}}$ distances ($2.3996(9)$ and $2.4039(9)\text{ \AA}$) are slightly elongated. The coordination geometry around zirconium was analysed with the help of the program SHAPE²⁸ and is best

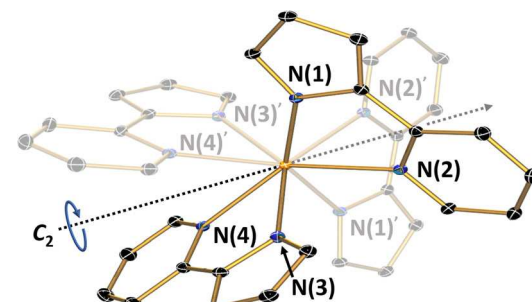


Fig. 1 Molecular structure of $\text{Zr}(\text{H}\text{PMPH})_4$ determined by X-ray crystallography. The symmetry-related ligands (transparent) are generated by the crystallographic C_2 axis passing through the zirconium centre.

described as a distorted triangular dodecahedron (TDD) (see ESI[†] for details), the most common eight-coordinate parent polyhedron.²⁹ Interestingly, the ^1H NMR spectrum shows only seven resonances, indicating higher symmetry in solution than in the C_2 -symmetric solid-state structure (Fig. S14, ESI[†]). This can be explained by considering a minor distortion to an S_4 -symmetric geometry, which renders all four ligands equivalent (Fig. 2). The small root-mean-square deviation (RMSD) of 0.26 \AA between the C_2 - and S_4 -symmetric structures highlights their remarkable similarity. The small energetic barrier expected for such a soft distortion precluded its observation by VT-NMR.

The electronic absorption spectrum of $\text{Zr}(\text{H}\text{PMPH})_4$ in dichloromethane (DCM) is shown in Fig. 3 and exhibits three strong, featureless absorption bands ($\varepsilon_{\lambda} > 20\,000\text{ M}^{-1}\text{ cm}^{-1}$). The lowest energy band ($\lambda_{\text{max}} = 380\text{ nm}$) is significantly red-shifted compared to that of the free ligand (Fig. S17, ESI[†]) indicating contributions from the metal centre to the frontier molecular orbitals. Absorption profiles recorded in solvents of varying polarity revealed a complete lack of solvatochromism (Fig. S18, ESI[†]), suggesting no significant change in dipole moment between ground and excited states. Time-dependent density functional theory (TD-DFT) calculations were carried out to elucidate the nature of the observed electronic

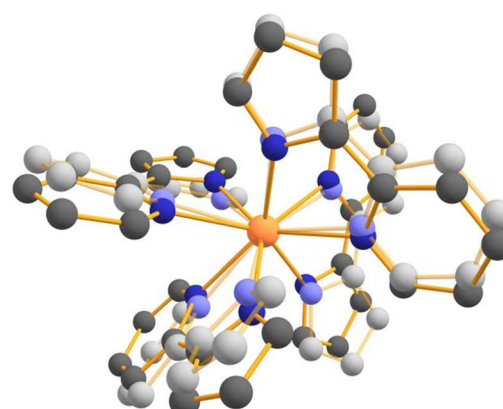


Fig. 2 Perspective view of the C_2 -symmetric crystal structure (bold) compared to the S_4 -symmetric structure (shaded) generated by Chem3D. The two structures have a root-mean-square deviation (RMSD) of 0.26 \AA which highlights their similarity.

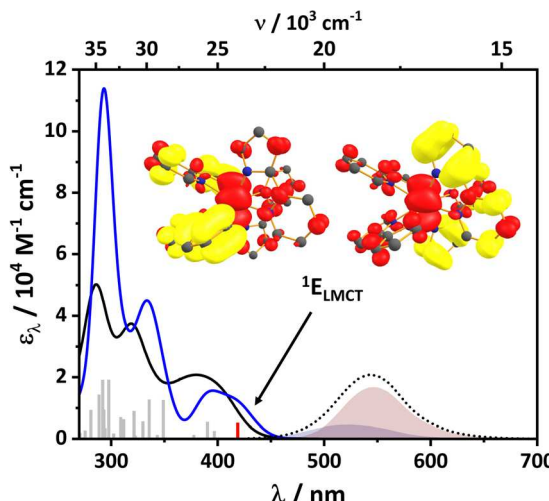


Fig. 3 Electronic absorption (solid black) and emission (dotted black) spectra of $\text{Zr}(\text{H}\text{PMPH})_4$ in dichloromethane. The TD-DFT calculated spectrum (solid blue, $\text{fwhm} = 2000 \text{ cm}^{-1}$) along with the predicted transitions (grey bars) are overlaid. The lowest energy ${}^1\text{LMCT}$ (${}^1\text{E}$) state is shown in terms of difference densities (red = gain of electron density, yellow = loss of electron density) with the corresponding TD-DFT transitions shown as red bars. The emission spectrum under air (transparent, navy) was subtracted from the spectrum under N_2 atmosphere (dotted black) to obtain the proposed phosphorescence spectrum (transparent, wine).

transitions, and satisfactory agreement with experiment was obtained using the B3LYP functional (Fig. 3). While no symmetry constraints were imposed during the calculations, effective S_4 symmetry (*vide supra*) is highlighted by the degeneracy of the S_1 and S_2 states within computational error ($\Delta E_{S_2-S_1} = 0.5 \text{ cm}^{-1}$) suggesting classification as a ${}^1\text{E}$ excited state. Inspection of the unrelaxed difference densities (Fig. 3) confirmed significant LMCT character in the lowest energy singlet excited states. A Mulliken population analysis of the unrelaxed densities of S_1 and S_2 (${}^1\text{E}$) shows significant negative charge migration to zirconium ($\Delta q = -0.36 \text{ e}$) when compared with the S_0 ground state, as expected for an LMCT transition. The delocalized nature of the ${}^1\text{E}$ excited state, involving equal contributions from all four ${}^1\text{H}\text{PDPH}^{1-}$ ligands, is consistent with the absence of an excited state dipole moment and the observed lack of solvatochromism.

Under N_2 atmosphere, excitation of the lowest energy absorption band results in a broad emission band ($\text{fwhm} = 2496 \text{ cm}^{-1}$) centred at 544 nm (Fig. 3). As for the absorption spectrum, no significant solvatochromism was observed for the emission profile (Fig. S19, ESI[†]). The photoluminescence quantum yield was measured to be 0.04 in DCM (Fig. S23 and S24, ESI[†]), a modest four-fold improvement over the previous PMP-based chromophores. Leveraging the stability of $\text{Zr}(\text{H}\text{PMPH})_4$, emission measurements in the presence of ${}^3\text{O}_2$ were conducted by exposing a DCM solution of the complex to air. The resulting steady-state emission spectrum revealed a significantly less intense, hypsochromically shifted band with a peak maximum at 521 nm (Fig. 3) consistent with partial luminescence quenching by ${}^3\text{O}_2$. This experiment suggests the presence of two distinct emission pathways in $\text{Zr}(\text{H}\text{PMPH})_4$ that were assigned as prompt fluorescence and phosphorescence. Due to the shift

in emission maximum upon exposure to air, a delayed fluorescence mechanism was dismissed because both prompt and delayed fluorescence are expected to emanate from the lowest-lying singlet excited state and should therefore have the same emission energy. Emission spectra recorded at 77 K in frozen solution (Fig. S20, ESI[†]) further support this assignment. Aside from more clearly resolved vibrational fine structure, the 77 K data show very little change when compared to the room temperature spectrum, which would be inconsistent with a thermally activated emission process.

Time-resolved emission measurements were conducted in DCM solution at room temperature (Fig. 4) and confirmed the presence of multiple emissive states with vastly different luminescence lifetimes for $\text{Zr}(\text{H}\text{PMPH})_4$. Rapid prompt fluorescence ($\tau_{\text{PF}} \leq 1 \text{ ns}$) manifests in a large initial drop of the emission intensity immediately following excitation. A second long-lived luminescence decay component with a lifetime of several hundred microseconds can be attributed to phosphorescence. Wavelength-dependent luminescence detection showed a more pronounced initial drop in the excited-state decay trace at shorter wavelengths than at longer wavelengths. These observations are fully consistent with the static emission spectra under N_2 and air (*vide supra*), based on which one would expect a larger

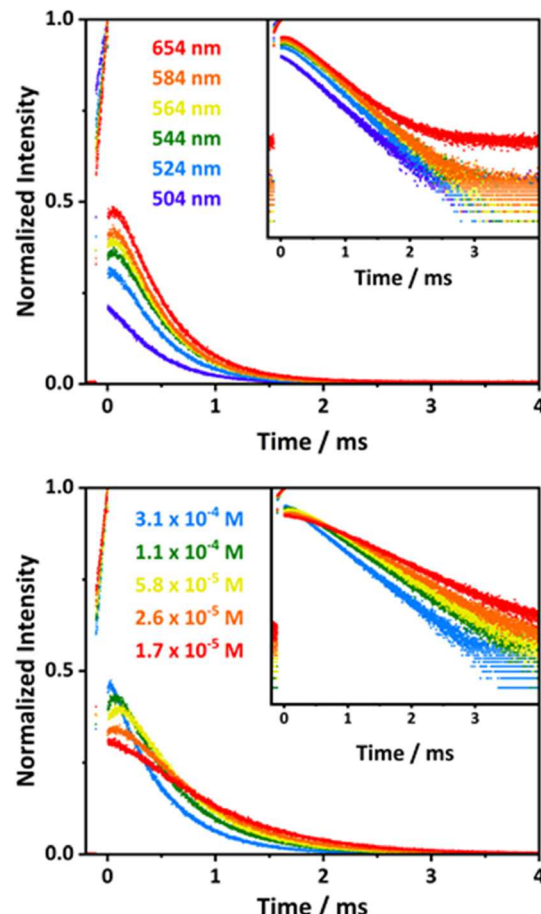


Fig. 4 Time-resolved emission data at variable detection wavelengths (top) and concentration (bottom). The insets show the data on a logarithmic scale.

contribution from fluorescence at shorter wavelengths and a larger contribution from phosphorescence at longer wavelengths. Complete disappearance of the long-lived feature in the presence of ${}^3\text{O}_2$ is fully consistent with spin-forbidden emission from a triplet excited state. The simultaneous observation of singlet and triplet emission suggests that intersystem crossing and prompt fluorescence are competitive processes that occur with similar time constants in $\text{Zr}({}^{\text{H}}\text{PMP}^{\text{H}})_4$.

Interestingly, the profile of the long-lived excited-state decay was dependent on the detection wavelength (Fig. 4, top). At longer wavelengths, a crest-like behaviour was observed where an initial rise in emission intensity is followed by simple monoexponential decay. Detection at a range of shorter wavelengths showed a gradual disappearance of this effect, accompanied by a slight increase in luminescence lifetime. This type of behaviour has been observed in aggregation-dependent emission processes such as excimer formation.^{30,31}

To gain further insight into potential diffusion-controlled processes, concentration-dependent measurements were conducted in DCM solution. The electronic absorption spectra (Fig. S21, ESI[†]) revealed no significant changes across two orders of magnitude in concentration (*ca.* 2×10^{-6} to 1×10^{-4} M), suggesting that aggregation in the ground state is unlikely to contribute to the observed optical properties. In contrast, the steady-state emission spectra (Fig. S22, ESI[†]) showed small but systematic changes across the same range of concentrations, reflected in a slight redshift and sharpening of the emission band. Additionally, time-resolved emission data (Fig. 4, bottom) displayed increasingly crest-like behaviour at higher concentrations. At the same time, the fitted time constant for the long-lived decay component decreased with increasing concentration, ranging from 793 μs for the most dilute sample to 473 μs for the most concentrated. While a complete understanding of the solution dynamics of $\text{Zr}({}^{\text{H}}\text{PMP}^{\text{H}})_4$ under visible light irradiation will require more detailed studies that are beyond the scope of this initial report, our experimental observations are consistent with excimer formation following photoexcitation. The intermolecular interactions seem to be relatively weak based on the small perturbations of the emission profiles but cause a significant reduction of the luminescence lifetime.

In conclusion, we have synthesized a novel, air- and moisture-stable zirconium(IV) complex which exhibits dual emission *via* prompt fluorescence and phosphorescence following excitation of an absorption band with significant LMCT character. A remarkably long photoluminescence lifetime of almost 800 μs was obtained in dilute solution, which minimizes the amount of excimer formation. To the best of our knowledge, $\text{Zr}({}^{\text{H}}\text{PMP}^{\text{H}})_4$ exhibits the longest photoluminescence lifetime of any early transition metal chromophore reported to date.

We thank the National Science Foundation (CHE-1752738) for financial support.

Conflicts of interest

The authors declare no conflicts of interest.

References

- 1 S. Zhang, X. Yang, Y. Numata and L. Han, *Energy Environ. Sci.*, 2013, **6**, 1443–1464.
- 2 H. Yersin, A. F. Rausch, R. Czerwieniec, T. Hofbeck and T. Fischer, *Coord. Chem. Rev.*, 2011, **255**, 2622–2652.
- 3 H. Xu, R. Chen, Q. Sun, W. Lai, Q. Su, W. Huang and X. Liu, *Chem. Soc. Rev.*, 2014, **43**, 3259–3302.
- 4 C. K. Prier, D. A. Rankic and D. W. C. MacMillan, *Chem. Rev.*, 2013, **113**, 5322–5363.
- 5 M. H. Shaw, J. Twilton and D. W. C. MacMillan, *J. Org. Chem.*, 2016, **81**, 6898–6926.
- 6 A. A. Yaroshevsky, *Geochem. Int.*, 2006, **44**, 48–55.
- 7 S. Otto, M. Dorn, C. Förster, M. Bauer, M. Seitz and K. Heinze, *Coord. Chem. Rev.*, 2018, **359**, 102–111.
- 8 O. S. Wenger, *J. Am. Chem. Soc.*, 2018, **140**, 13522–13533.
- 9 C. Wegeberg and O. S. Wenger, *JACS Au*, 2021, **1**, 1860–1876.
- 10 C. Förster and K. Heinze, *Chem. Soc. Rev.*, 2020, **49**, 1057–1070.
- 11 W. Gawelda, A. Cannizzo, V.-T. Pham, F. van Mourik, C. Bressler and M. Chergui, *J. Am. Chem. Soc.*, 2007, **129**, 8199–8206.
- 12 P. Chábera, K. S. Kjaer, O. Prakash, A. Honarfar, Y. Liu, L. A. Fredin, T. C. B. Harlang, S. Lidin, J. Uhlig, V. Sundström, R. Lomoth, P. Persson and K. Wärnmark, *J. Phys. Chem. Lett.*, 2018, **9**, 459–463.
- 13 J. D. Braun, I. B. Lozada, C. Kolodziej, C. Burda, K. M. E. Newman, J. Van Lierop, R. L. Davis and D. E. Herbert, *Nat. Chem.*, 2019, **11**, 1144–1150.
- 14 L. A. Büldt, X. Guo, R. Vogel, A. Prescimone and O. S. Wenger, *J. Am. Chem. Soc.*, 2017, **139**, 985–992.
- 15 C. Wegeberg, D. Häussinger and O. S. Wenger, *J. Am. Chem. Soc.*, 2021, **143**, 15800–15811.
- 16 P. Herr, C. Kerzig, C. B. Larsen, D. Häussinger and O. S. Wenger, *Nat. Chem.*, 2021, **13**, 956–962.
- 17 M. S. Lazorski and F. N. Castellano, *Polyhedron*, 2014, **82**, 57–70.
- 18 B. W. Pfennig, M. E. Thompson and A. B. Bocarsly, *J. Am. Chem. Soc.*, 1989, **111**, 8947–8948.
- 19 G. V. Loukova, W. Huhn, V. P. Vasiliev and V. A. Smirnov, *J. Phys. Chem. A*, 2007, **111**, 4117–4121.
- 20 C. Romain, S. Choua, J. P. Collin, M. Heinrich, C. Bailly, L. Karmazin-Brelot, S. Bellemain-Laponnaz and S. Dagorne, *Inorg. Chem.*, 2014, **53**, 7371–7376.
- 21 Y. Zhang, J. L. Petersen and C. Milsmann, *J. Am. Chem. Soc.*, 2016, **138**, 13115–13118.
- 22 Y. Zhang, D. C. Leary, A. M. Belldina, J. L. Petersen and C. Milsmann, *Inorg. Chem.*, 2020, **59**, 14716–14730.
- 23 Y. Zhang, T. S. Lee, J. M. Favale, J. L. Petersen, G. D. Scholes, F. N. Castellano and C. Milsmann, *Nat. Chem.*, 2020, **12**, 345.
- 24 M. Yang, S. Sheykhi, Y. Zhang, C. Milsmann and F. N. Castellano, *Chem. Sci.*, 2021, **12**, 9069–9077.
- 25 Y. Zhang, N. G. Akhmedov, J. L. Petersen and C. Milsmann, *Chem. – Eur. J.*, 2019, **25**, 3042–3052.
- 26 Y. Rong, A. Al-Harbi and G. Parkin, *Organometallics*, 2012, **31**, 8208–8217.
- 27 P. M. N. Đô, N. G. Akhmedov, J. L. Petersen, B. S. Dolinar and C. Milsmann, *Chem. Commun.*, 2020, **56**, 5397–5400.
- 28 M. Pinsky and D. Avnir, *Inorg. Chem.*, 1998, **37**, 5575–5582.
- 29 D. Casanova, M. Llunell, P. Alemany and S. Alvarez, *Chem. – Eur. J.*, 2005, **11**, 1479–1494.
- 30 J. B. Birks, D. J. Dyson and I. H. Munro, *Proc. R. Soc. London, Ser. A*, 1963, **275**, 575–588.
- 31 O. P. Dimitriev, Y. P. Piryatinski and Y. L. Slominskii, *J. Phys. Chem. Lett.*, 2018, **9**, 2138–2143.